Surfaces and Interfaces 69 (2025) 106800

Contents lists available at ScienceDirect

Surfaces and Interfaces

journal homepage: www.sciencedirect.com/journal/surfaces-and-interfaces

Tannic acid loading into polyurethane and epoxy coatings: Active corrosion protection of AA2024 alloy

Rubén del Olmo [a,b,*], Cristina Neves [a], Alexandre Bastos [a], Raúl Arrabal [b], João Tedim [a]

[a] CICECO, Dep. Materials and Ceramic Engineering, University of Aveiro, 3810-193, Aveiro, Portugal
[b] Department of Chemical and Materials Engineering, Faculty of Chemical Sciences, Complutense University of Madrid, 28040, Madrid, Spain

ARTICLE INFO

Keywords:
Aluminium alloy
Layered double hydroxides
Tannic acid
Polyurethane coating
Epoxy coating
Green corrosion inhibitor
Active corrosion protection

ABSTRACT

Driven by the recent discovery of tannic acid (TA) as an effective green corrosion inhibitor for AA2024 alloy, this study evaluates its suitability as an additive for epoxy (EP) and polyurethane (PU) coatings, both through direct addition and by immobilization into layered double hydroxides (LDH-TA). LDH-TA was characterized by XRD, FTIR, and UV-visible spectrophotometry. Also, its anticorrosion performance was evaluated using EIS. The results show that the direct addition of TA to EP and PU coatings reduces their barrier properties, whereas incorporating LDH-TA into the polyurethane matrix provides superior corrosion protection compared to the epoxy coating. Therefore, LDH-TA-loaded PU coating (PU-LDH-TA) was further characterized through rheology analysis, surface characterization, release studies, and electrochemical techniques (EIS and SVET). The findings indicate that after 28 days, $|Z|$ at 10^{-2} Hz for PU-LDH-TA remains over one order of magnitude higher than PU. Besides, upon coating defects, tannate anions released from the polyurethane coating form a protective Al/tannate-rich hydroxide layer at the defect site. Thus, PU-LDH-TA demonstrates effective active corrosion protection in saline media while maintaining the structural integrity of the coating.

1. Introduction

To date, the aircraft industry still faces a significant challenge in seeking eco-friendly and efficient chromate-free surface treatments for aluminum alloys. Specifically, among the used Al alloys in commercial aircraft, considerable attention has been directed toward AA2024-T3 alloy (Al-Cu system) due to its exceptional specific mechanical properties [1,2]. Unfortunately, its susceptibility to localized corrosion has required the use of a Cr-based multilayered protection scheme, which includes a pre-treatment layer (anodic or conversion film) followed by epoxy primer and polyurethane topcoat layers [1,3,4].

The search for Cr-free alternatives is being driven by the European Chemicals Agency (ECHA), as Cr-based compounds for surface treatments and organic coatings have been classified as substances of very high concern (SVHC), due to their high toxicity and carcinogenic properties to humans and aquatic life [4,5]. In response, the aircraft industry has invested over €100 million to find efficient and cost-effective Cr-free surface treatments (including conversion and organic coatings) for aluminum alloys. However, the lack of suitable alternatives underscores the need for alternatives with a similar performance to that of chromates [1,5].

In this context, the ideal Cr-free coating should provide active corrosion protection, *i.e.*, when a Cr-based coating undergoes corrosion and/or physical damage, Cr(VI) derived species are released to interact with the exposed alloy [6]. This process involves the precipitation of protective compounds, usually triggered by pH changes on the anodic/cathodic regions of the AA2024 alloy [1,5,6].

A recently explored approach to avoid the use of Cr-based surface treatments involves incorporating various corrosion inhibitors into epoxy and polyurethane formulations. Examples include lithium [7] and cerium (III) salts [8], as well as organic compounds such as 8-hydroxyquinoline, salicylaldimine, and 2,5-dimercapto-1,3,4-thiadiazolate [9,10]. However, while some of these inhibitors provide active protection, a notable drawback is their effectiveness only at relatively high concentrations (~ 1 wt.%). Furthermore, although less toxic than chromates, most of these corrosion inhibitors are still considered harmful, with long-lasting detrimental effects on humans and aquatic life [11].

Based on this premise, the present work adopts the fundamental hypothesis derived from a recently published work by our group [12]. In that study, we demonstrated that saline solutions of tannic acid (a cost-effective and natural product), efficiently formed a tannate-rich corrosion protective layer on the AA2024 alloy. Notably, the results

* Corresponding author.
E-mail address: rubandom@ucm.es (R. del Olmo).

https://doi.org/10.1016/j.surfin.2025.106800
Received 18 March 2025; Received in revised form 17 May 2025; Accepted 25 May 2025
Available online 26 May 2025

indicated the highest corrosion performance at minimal concentrations (0.1-1 mM). This concentration-sensitive inhibition is a critical feature, as the direct incorporation of a corrosion inhibitor into a polymeric matrix may negatively impact its rheological and structural properties, especially at high concentrations [13,14]. Although this concern has been scarcely addressed in the available literature, recent studies have explored different strategies to encapsulate corrosion inhibitors [14–16]. Among the different encapsulation reservoirs reported for organic corrosion inhibitors [16,17], including mesoporous silica [16, 18], halloysite [19,20], zeolites [21], and polymeric capsules [15,17, 22], the use of layered double hydroxides (LDHs) stands out [23–26]. LDH are hydrotalcite-like containers composed of positively charged metal hydroxide layers capable of intercalating anionic species, including organic anions [27]. Additionally, LDHs have been studied for drug delivery in biomedicine due to their low toxicity, high biocompatibility, cost-effectiveness, and ability to provide controlled release of corrosion inhibitors [28–30].

To the best of the authors' knowledge, the available literature does not address the suitability of tannic acid, either as a stand-alone agent or immobilized in LDHs, in water-based epoxy and polyurethane coatings applied on AA2024 alloy.

Therefore, this study aims to evaluate, for the first time, the compatibility of stand-alone and tannic-containing LDH additives in commercial and water-based epoxy and polyurethane formulations. The coatings demonstrating the most promising performance in terms of surface appearance and short-term corrosion resistance are subjected to comprehensive evaluation. This analysis encompasses (i) rheological properties; (ii) surface characterization through optical profilometry, Fourier-transform infrared spectroscopy (FTIR), water contact angle measurements, and scanning electron microscopy (SEM); (iii) the release dynamics of tannate anions from the LDH additive and the formulated coatings; (iv) long-term corrosion resistance assessed via electrochemical impedance spectroscopy (EIS); and (v) active protection performance by the scanning vibrating electrode technique (SVET).

2. Methodology

2.1. Chemicals

Tannic acid (purity: ≥ 99 %), hereinafter referred to as "TA", and sodium chloride (purity: ≥ 99 %) were acquired from Sigma-Aldrich, whereas Zn-Al/NO_3 LDH (Zn/Al=2; water-based slurry), hereinafter referred to as "LDH", was produced by Smallmatek Lda and used as received. The following coating components were acquired from SYNPO (akciová společnost, Czechia): acrylic polyurethane AQ CC 80 and hardener AQ BU; water-based epoxy V2205 and hardener V7003.

2.2. Pre-treatment of AA2024 substrate

Before applying the epoxy and polyurethane coatings, rectangular 100 mm × 75 mm × 2 mm specimens of commercial 2024-T3 alloy (wt. %: 3.8–4.9 Cu, 1.2–1.8 Mg, 0.3–0.9 Mn, < 0.5 Fe, < 0.5 Si, < 0.25 Zn, < 0.15 Ti, < 0.10 Cr and Al balance) were chemically etched following a three-step industrial cleaning procedure consisting of etching in a 48 g/L METACLEAN T2001 solution for 15 min at 65°C and in a 65 g/L TURCO LIQUID ALUMINTECH for 45 s at 60°C. Each procedure was followed by stirring (300 rpm) and cleaning with deionized water. The specimens were then desmutted in a 180 mL/L BONDERITE C-IC SMUTGO NC AERO solution for 7 min at 25 °C. Finally, all plates were rinsed in distilled water, and dried with warm air.

2.3. Tannic-loading into layered double hydroxide additive: intercalation, characterization, corrosion performance, and release studies

Tannate anions were immobilized in LDH (hereinafter referred to as "LDH-TA") by a one-step ion exchange process. The synthesis was performed by dispersing 13 g Zn-Al-NO_3-LDH slurry (solid content: 7 wt %) in 100 mL of 0.1 M tannic acid solution at different pH values (6, 8, and 10) under vigorous stirring for 6 hours at 50 °C. Since TA is a weak acid (pKa ~ 6), the intercalation of tannate anions into the host LDH was carried out at different pH values to check the best value for the intercalation of tannate anions. The resulting brownish slurry was then rinsed with deionized water and centrifuged 3 times to remove any residues. The cleaned LDH-TA slurry was dried for 4 hours at 80°C, and the dried resulting material was ground into a fine powder.

The stand-alone TA and LDH-TA powders were analyzed via Attenuated Total Reflectance Fourier Transform Infrared (ATR-FTIR) spectrometry using a Bruker Optics Fourier Transform-IR spectrometer equipped with a Golden Gate ATR accessory plate. FTIR spectra were recorded over the 4000 to 400 cm^{-1} range with a resolution of 2 cm^{-1}. The crystalline structure of the TA, LDH and LDH-TA dried powders was examined by X-ray diffraction (XRD) using an XPert PRO3 (Malvern Panalytical) diffractometer with Cu Kα radiation (λ = 1.5418 Å) and a graphite monochromator. To assess the corrosion performance of the LDH-TA additive, cleaned AA2024 alloy specimens were immersed in a 3.5 wt.% NaCl solution containing the LDH-TA additive in suspension (0.01 wt.%) synthesized at pH 6, 8, and 10. Electrochemical impedance spectroscopy (EIS) measurements were conducted under the same conditions as those used for evaluating the studied coatings (refer to *Section 2.6.1*).

To investigate the kinetics of tannate release from the LDH-TA additive, 80 mg of the LDH-TA powder (synthesized at pH 10) was dispersed in 80 mL of a 3.5 wt.% NaCl solution under continuous stirring (300 rpm). Note that pH 10 was chosen to ensure the most tannate immobilization/intercalation (for further information, see *Section 3.1*). Aliquots were extracted at various time intervals (0-7 days) using a syringe and filtered through PTFE membrane filters (0.45 μm pore size) for UV-visible analysis. After each measurement, the aliquot was placed again in the immersion solution to continue the tannate release process (LDH particles retained in the filter were not taken into account due to their negligible content). The loading content of the tannate anions in the LDH-TA powder was determined by dissolving a known amount of powder in a 0.1 M HNO_3 aqueous solution. After 5 minutes of stirring, the aliquots (in triplicate) were filtered through PTFE membrane filters (0.45 μm pore size) and analyzed using UV-visible spectroscopy. The immobilized/intercalated content of tannate anions on LDH (pH 10) was determined to be 72 ± 5 wt.%.

2.4. Preparation and application of the epoxy- and polyurethane-based coating formulations on AA2024 alloy

Commercial water-based acrylic polyurethane emulsion (hereinafter referred to as "PU" in the manuscript), AQ CC 80 (35 wt.% solid content), and epoxy primer V2205 (hereinafter referred to as "EP" in the manuscript) were used for the coating preparation. These formulations were chosen due to their lower content of volatile organic compounds (VOC) compared to conventional solvent-based formulations. TA and LDH-TA powders were added into both EP and PU formulations at concentrations ranging from 0 to 0.5 wt.% for TA and 0.1 wt.% for the LDH-TA additive. TA and LDH-TA powders were dispersed in EP and PU formulations using magnetic stirring at 300 rpm for 1 hour, followed by ultrasound treatment for approximately 1 h. Then, the corresponding coating hardeners were added carefully to the formulations and stirred for 10 minutes. The resin-to-hardener ratios were 2.5:1 for PU and 7:1 for EP formulations. Coatings were then applied using a gap film applicator with a slit thickness of 150 μm, resulting in varied dry film thicknesses depending on the formulation used (described in the results section).

2.4.1. Compatibility of the LDH-TA powder with the coating formulation: rheological studies

As the PU system demonstrated the most promising results in

preliminary assessments (*Section 3*), rheological analysis was focused exclusively on this system. Namely, the influence of LDH-TA on the performance of PU-based coatings was analyzed in terms of viscosity and viscoelastic behaviour following a similar procedure described in [13,14]. For that, a Kinexus lab + rotational rheometer (Malvern), equipped with a 4° cone geometry with a 40 mm diameter and a 150 μm gap (CP4/40 SR2216 SS), was employed for the rheological measurements. The viscosity analysis was carried out through a shear rate sweep ranging from 1 to 1000 s^{-1} (10 points per decade). Additionally, yield stress assessment was performed by a shear stress ramp from 0.1 to 100 Pa (10 points per decade). To address the viscoelastic properties, a constant shear strain of 2% was applied during a frequency sweep from 1 to 10 Hz (10 points per decade). The linear viscoelastic region was ascertained after performing an amplitude sweep, where shear stress ranged from 0.1 to 10 Pa (at 1 Hz; 10 points per decade). All rheological tests were conducted at 25°C.

2.5. Characterization of the EP and PU-based coatings on AA2024 alloy

Visual inspection of EP- and PU-coated AA2024 samples before and after exposure to a 3.5 wt.% NaCl solution was monitored over time using an optical microscope (Nikon SMZ18 microscope).

The thickness of the studied coatings was determined using an ISO SCOPE FMP10 eddy current meter (Fischer) equipped with an FTA3.3H probe. The obtained values were further confirmed by optical microscopy. Cross-sections were prepared by embedding in MA2+ commercial EP resin (Sigma-Aldrich) and using successive grades of silicon carbide abrasive papers ranging from P120 to P1200.

Dry adhesion of PU-coated specimens was evaluated following the ISO 2409 standard. The rating system of this standard is based on the detached surface area (%) after the test (rating 0: no detachment; rating 5: complete detachment).

Topographic 2D and 3D images were obtained with an InfiniteFocusSL optical profilometer (ALICONA, GmbH) to determine roughness and texture differences in PU coatings on AA2024 alloy. Topographic information was analyzed with the IF-Measure Suite software to extract roughness parameters, such as Ra (arithmetic mean value in a roughness profile) and Sa (the difference in height of each point compared to the arithmetical mean of the surface).

FTIR analysis of PU-coated AA2024 alloy samples was conducted under the same conditions described in *Section 2.3*. In this case, the coatings were analyzed as separate films by applying the coating formulations on Teflon substrates and peeling them off (Fig. 1).

The wettability of PU-based coatings on AA2024 was evaluated using deionized water with an Attension Theta tensiometer (Biolin Scientific) and the Oneattension software. The Laplace-Young method was used to determine the contact angle, with reported values representing the average of 6 drops (3 droplets on two replicate specimens).

2.5.1. Release studies of the Tannate anions from PU coating

For the release studies of the LDH-TA additive from the PU coating, the coating was first applied onto Teflon substrates and peeled off. Then, 10 g of PU coating loaded with LDH-TA additive was immersed in 100 mL of a 3.5 wt.% NaCl solution under stirring at 300 rpm. At different time slots (0-7 days), aliquots were extracted from the suspension using a syringe and filtered through PTFE membrane filters with a pore size of 0.45 μm for UV-visible analysis (as described in *Section 2.3*). After each measurement, the aliquot was returned to the immersion solution (LDH particles retained in the filter were not taken into account due to their negligible content). **Figure S1** summarises this process for ease of understanding.

2.6. Corrosion evaluation of the studied EP- and PU-based coatings on AA2024 alloy

2.6.1. Electrochemical impedance spectroscopy (EIS)

EIS was performed to evaluate the corrosion resistance of EP- or PU-coated AA2024 alloy specimens. The coated AA2024 specimens, with an exposed area of 3.4 cm^2, were placed in a three-electrode configuration connected to a Gamry potentiostat/ZRA 1000 interface. A saturated calomel electrode (SCE) served as the reference electrode, while a platinum foil acted as the counter electrode. EIS spectra were recorded at open circuit potential (OCP) after different immersion times (up to 28 days) in 3.5 wt.% NaCl solution (pH: 6.6 ± 0.2) at room temperature. The frequency range was from 10^5 Hz to 10^{-2} Hz, with a sinusoidal amplitude (RMS) of 10 mV and 7 points per decade. All measurements were performed in triplicate within a Faraday cage to ensure repeatability. For data analysis, impedance spectra were fitted using appropriate equivalent circuits with the *Gamry Echem Analyst* software. The ideal capacitance was calculated using equation (1) for the CPE-coat and CPE-ox, and Equation (2) for CPE-dl, as will be stated in the used equivalent circuits disclosed in *Section 3.4.1*. C is the capacitance, and Q (admittance) and n are the CPE parameters. Rf is the resistance of a specific film, and Rsol is the solution resistance (ohmic resistance) [31].

$$C = Q^{1/n}\ Rf^{(1-n)/n} \tag{1}$$

$$C = Q^{1/n}\left(\frac{Rsol\ Rf}{Rsol + Rf}\right)^{(1-n)/n} \tag{2}$$

The goodness of fit was guaranteed by chi-square values less than 0.01 (the square of the standard deviation between the original data and the calculated spectrum).

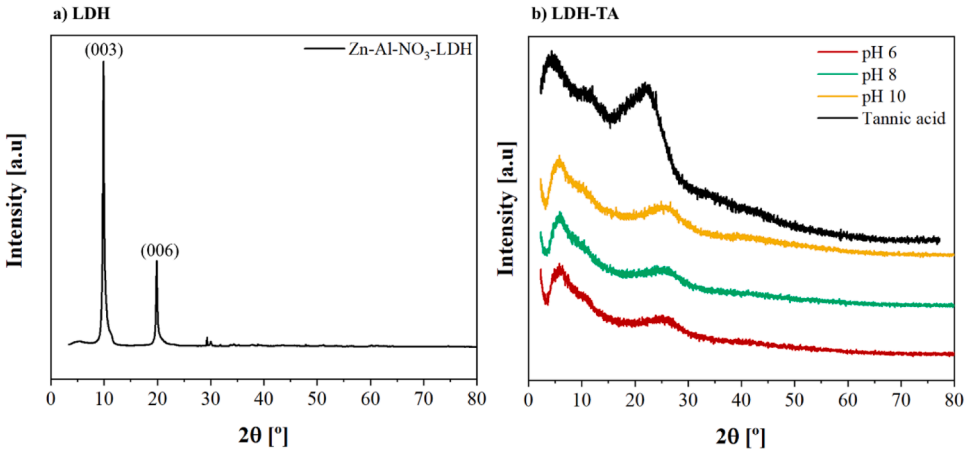

Fig. 1. X-ray diffraction patterns of the (a) stand-alone LDH, and (b) LDH-TA powders.

2.7. Active corrosion protection of the studied polyurethane coatings on AA2024 alloy

2.7.1. Visual observation and defect characterization

PU-coated AA2024 specimens, both with and without LDH-TA additive, were manually scribed with a surgical blade, ensuring that the scribe penetrated through the coating to expose the underlying substrate. Subsequently, these specimens were immersed in an aqueous 3.5 wt% NaCl solution for 7 days. The scribes were monitored by scanning electron microscopy (SEM, Hitachi SU-70, 15.0 kV). The chemical composition of the surface defects was analyzed using energy dispersive spectroscopy (EDS). Note that no additional coating (gold and/or carbon) was applied to the analyzed defects to better quantify the composition of the defect.

2.7.2. EIS analysis on defect coatings

To evaluate the active corrosion protection capability of the studied systems, PU-coated specimens were manually damaged using a medical needle (the depth of the point-shaped defect was larger than the coating thickness and reached the underlying substrate). Afterwards, EIS tests and SEM/EDS analyses were performed after 7 days of immersion, following the same procedure described in *Section 2.6.1* and *2.7.1*, respectively.

2.7.3. SVET analysis

Selected PU-based coatings (4 × 4.5 mm^2) were subjected to SVET analysis to quantify ionic currents in a 0.05 M NaCl solution and assess their self-healing performance. Each coating sample had two point-shaped defects made with a medical needle, and measurements were conducted 100 μm above the sample surface. The testing area was delimited by beeswax to prevent any corrosion activity outside the tested area. The measurements were performed with equipment from Applicable Electronics Inc. (USA) using the ASET software from Science Wares Inc. (USA), equipped with a Pt-Ir microelectrode (insulated with Parylene C; www.microprobes.com, USA). A 40 μm diameter sphere of platinum black was deposited at the tip. The microelectrode vibrated with frequencies of 65 Hz and 108 Hz in the normal and parallel directions to the surface with 10 μm amplitude in both directions. Each map comprised 50 × 50 points. The SVET maps presented here only show the z component (current flowing perpendicularly to the surface). For further experimental details, the reader is referred to [32,33].

3. Results and discussion

Given that both EP and PU resins are used in multilayer systems for AA2024 alloys, the first approach is to ascertain, rather than compare, the suitability of tannic acid (TA) as corrosion inhibitor in both resins. As a first approach, the direct incorporation of TA into EP and PU coatings (**Figure S2, S3**) was evaluated in terms of corrosion resistance by EIS after 7 days of immersion in 3.5 wt.% NaCl. Additionally, to qualitatively assess their possible active corrosion performance, scribed coatings were also tested.

In EP coatings (**Figure S2**), the intact and scribed EP reference coating exhibited the highest barrier properties, indicating that the incorporation of TA negatively affects its corrosion performance. Since the coating thickness was comparable in all EP coatings (33 ± 4 μm), the lower corrosion performance may be attributed to the presence of intermolecular hydrogen bonds, van der Waals interactions, and π-π stacking of the aromatic rings in TA, which is known to promote the precipitation of tannate products in similar epoxy-based formulations [34].

In contrast, the presence of small amounts of TA (0.1–0.25 wt.%) in PU coatings enhanced the corrosion performance compared to higher concentrations (0.5 wt.%) (Figure S3). However, scribed TA-loaded PU coatings exhibited greater delamination than the PU reference coating. This may be associated with the hygroscopic nature of the PU coating [35].

Therefore, given the low performance of the stand-alone incorporation of tannic acid into EP and PU coatings, tannic acid was incorporated into LDH powder (hereinafter referred to as LDH-TA).

3.1. Characterization, corrosion performance and release studies of LDH-TA powder

Prior to the incorporation of LDH-TA into the Epoxy and PU coatings, the synthesized LDH-TA powder was characterized to assess its structural, morphological, and tannate release performance. Fig. 1 shows the XRD patterns of the reference LDH ($ZnAl\text{-}NO_3$) and the LDH-TA powders as a function of the used pH values (6, 8, and 10) during TA loading.

The XRD pattern in Fig. 1**a** reveals the presence of the (003) and (006) characteristic reflections, thus confirming the intercalation of nitrates in the LDH galleries [36,37]. Nevertheless, following the tannate exchange step, the LDH reflections were not detected (Fig. 1**b**). Comparing the different LDH-TA with TA itself, it is clear that the XRD pattern of LDH-TA has similarities with TA XRD pattern, which can be associated with significant amounts of TA adsorbed on LDH.

Furthermore, if some anion-exchange between nitrates and TA would occur, the large molecular size TA could influence the structural ordering in LDH, ultimately leading to the decrease of peak intensity at low 2θ angles ascribed to LDH structure. This decrease in intensity of XRD peaks has been previously reported in the literature after anion exchange between nitrate and vanadate or MBT in Zn–Al LDHs [38,39]. In the present study, this effect may be even more noticeable due to the significantly larger molecular size of TA compared to the anions utilized in those studies. Therefore, from XRD analysis, it is not possible to conclude that TA is immobilized inside LDH galleries.

Regarding LDH morphology, complementary SEM images of LDH and LDH-TA powders along with the EDS analysis of LDH-TA powder (**Figure S4**) show that the LDH plate-like morphology is retained upon anion-exchange reaction (pH 10). However, the small irregular domains observed on the LDH-TA surface cannot be conclusively identified as pure TA or small LDH particles, as TA is composed of C and O, and EDS mapping does not allow for accurate carbon detection from TA on the surface.

To further characterize the interaction of tannate anions with the layered double hydroxides, both LDH and LDH-TA powders were analyzed by FTIR (Fig. 2). In the case of LDH (Fig. 2**a**), the broad absorption band around 3400 cm^{-1} corresponds to the stretching vibrational mode of O-H in water molecules and LDH structure. The small band at ~1650 cm^{-1} corresponds to the bending of the interlayer water molecules [40,41]. The bands located at 1350 cm^{-1} and 400-650 cm^{-1} correspond to vibrations associated with NO_3^- anions and M-O, M-OH (M=Zn, Al) stretching bond vibrations [36,40,42,43], respectively.

In the case of LDH-TA powder (Fig. 2**b**), the decrease in the intensity of the O-H band at 3500-3000 cm^{-1} compared to tannic acid, may be attributed to the deprotonation of tannic acid into tannates, regardless of the pH value used in the ion exchange process. Additionally, the bands occurring between 1050-900 cm^{-1} (C-O-C) and 1740-1520 cm^{-1} (C=C) can be associated with the presence of tannates [44,45]. As shown in XRD analysis, since the LDH-TA FTIR spectrum resembles that of tannic acid, it can be inferred that tannate anions are present in LDH, most likely adsorbed on LDH in large amounts to mask LDH signals [40]. This is in line with the high-loading content of TA (72 ± 5 wt.%.) determined and described in *Section 2.3*.

The corrosion performance of LDH-TA prepared under different pH conditions was additionally evaluated by EIS for AA2024 alloy exposed to 3.5 wt.% NaCl solution, after 7 days of immersion (Fig. 3). Compared to the NaCl reference solution, the presence of dispersed LDH-TA (0.01 wt.%) in the NaCl solution increases the impedance modulus by an order of magnitude over the intermediate and low frequency ranges, where the corrosion processes are expected to occur (Fig. 3**a**). Furthermore, the absence of corrosion products in all LDH-TA-containing solutions and

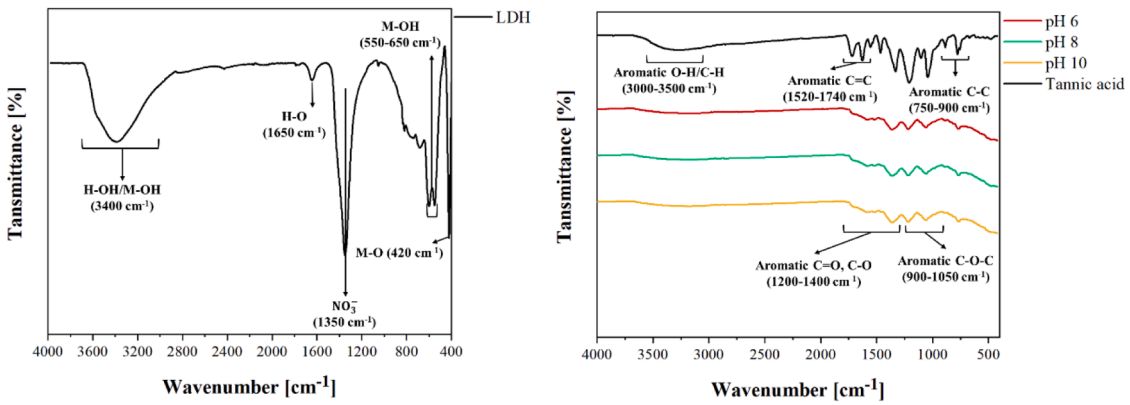

Fig. 2. FTIR spectra of (a) LDH, and (b) LDH-TA powders synthesized at pH 6, 8, and 10.

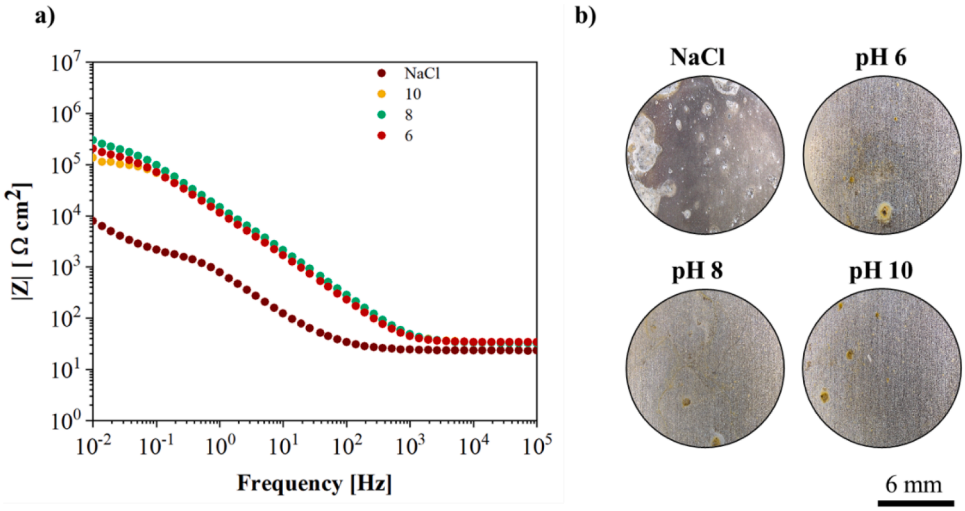

Fig. 3. (a) Bode representation of EIS spectra (only impedance magnitude is depicted) and (b) visual inspection of AA2024 alloy after 7 days of immersion in 3.5 wt. % solution in the presence of LDH-TA powder (0.01 wt.%) synthesized at different pH values (6, 8, 10).

the presence of tannate precipitates/passivated pits [12] indicates that the synthesis pH of LDH-TA powder has a negligible effect on its corrosion performance (Fig. 6**b**).

In this scenario, since no significant differences were found for LDH-TA powder prepared at different pH, the tannic loading process was performed at pH 10 to ensure that the highest amount of free tannate anions was available to interact with the LDH structure (*Section 2.3*). To study the release of tannate anions from the LDH structure, the cumulative release profile (Q) and the concentration of tannate anions per gram of LDH powder in 1 L of 3.5 wt.% NaCl solution was analyzed at different immersion times (Fig. 4).

As evidenced by the Q-cumulative release profile (Fig. 4**a**) and the concentration profile of tannate anions (Fig. 4**b**), a burst release of tannate anions from the LDH powder occurs immediately after

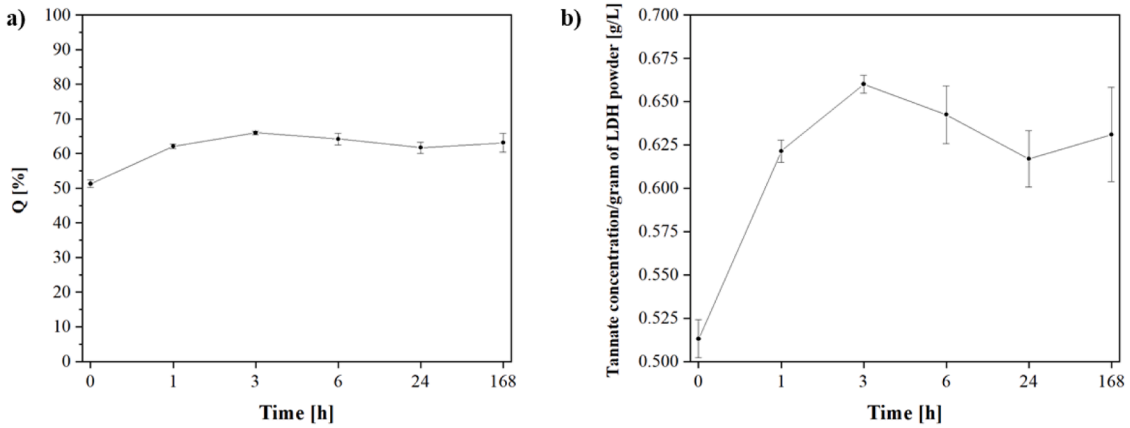

Fig. 4. (a) Q-cumulative release profile, and (b) concentration of released tannate anions per gram of LDH powder in 3.5 wt.% NaCl solution at different times (error bars are standard deviation of 3 replicas).

dispersing LDH-TA powder in the saline solution. This may correspond to fast desorption of the excess adsorbed tannate anions available in the LDH surface (Fig. 4**b**).

Since the desorption level of tannates is below their solubility limit in water (~250 g L^{-1}; CAS: 1401-55-4), it can be stated that not all of the adsorbed TA was fully released upon contact with the NaCl solution. Therefore, the release of TA cannot be solely attributed to spontaneous leaching driven by a reversible desorption process but is likely influenced, in part, by a dynamic anion-exchange equilibrium between tannates and chlorides [31]. These results confirm that a portion of the tannate is intercalated within the LDH structure, further supporting the constant release of tannate anions through the anion exchange process.

As the immersion time progresses, the release of TA from LDH stabilizes after 3-4h, which is in agreement with the release profiles observed for other organic compounds such as MBT [46]. Interestingly, after the first 3 hours of immersion, a slight decrease in the Q-cumulative release values and the concentration of released tannate anions were observed till the end of the test (Fig. 4). These fluctuations can be due to the re-adsorption of the released tannate anions on the surface of LDH, as shown in other release profiles of organic anions from similar LDHs [31,46].

3.2. Compatibility of LDH-TA into EP and PU coatings

Therefore, given the low performance of the stand-alone incorporation of tannic acid in both formulations (**Figures S2, S3**), the corrosion performance assessment of the LDH-TA powder as an additive in EP and PU coatings was conducted as described in *Section 3*.

As can be seen in Fig. 5**a**, the reference EP coating revealed a higher impedance modulus over the entire frequency range and better surface appearance before and after the artificial scribe compared to the LDH-TA-loaded EP coating (referred to hereafter as PU-LDH-TA coating). Given the immobilization of TA in layered double hydroxides and its release performance in saline medium (Fig. 4), the release of some TA into the water-based EP and PU coating formulations may explain the colour change of the reference coatings. Therefore, the poor interaction between LDH-TA and EP (Fig. 5**a**) aligns with the previously discussed precipitation of tannates in the epoxy matrix, as previously stated in *Section 3*. These observations contrast with the available literature, where the incorporation of organic-loaded LDH (2-MBT [47,48], gallic [49], and aromatic compounds [50], among others) usually improves the barrier properties and dispersion of LDH in EP formulations.

Conversely, the presence of the LDH-TA additive in the PU coating (referred to hereafter as PU-LDH-TA coating) results in a coating with equivalent, slightly improved impedance, without visible corrosion activity on both intact as well as scribed coatings (Fig. 5**a, b**). This finding aligns with existing studies that focus on incorporating organic-modified LDH additives into polyurethane resins [51,52]. These studies reported enhanced mechanical properties, adhesion, and thermal stability of the polyurethane matrix due to the interaction between the hydroxyl groups of the functionalized LDH powders and the polar groups of the polyurethane resin [52–54]. In the present study, this interaction may occur between the hydroxyl groups from the tannate anions (released and adsorbed) with the water-based polyurethane formulation.

Based on these results, we can state that TA is only compatible with PU resin used in the present study, when immobilized as LDH-TA. Therefore, PU-LDH-TA and PU coatings were selected for further characterization and corrosion studies, as will be described in the following sections.

3.3. Surface characterization PU and PU-LDH-TA coatings: rheology, surface properties, and release studies

3.3.1. Rheological studies of PU and PU-LDH-TA formulation

The rheological studies (Fig. 6) aim to ascertain the effect of the LDH-TA additive on the viscosity and viscoelastic behaviour of the PU formulation.

Concerning the rotational rheology (Fig. 6**a**), the addition of 0.1 wt. % LDH-TA to the PU formulation results in a similar viscosity to that of the original PU formulation across all shear rate values (1-1000 s^{-1}). Both formulations exhibit nearly constant viscosity over a wide shear rate range, with values stabilizing around 0.01-0.015 Pa.s. This behaviour denotes that the water content of the PU formulation ensures good LDH-TA dispersion, likely due to hydration effects, thereby preventing

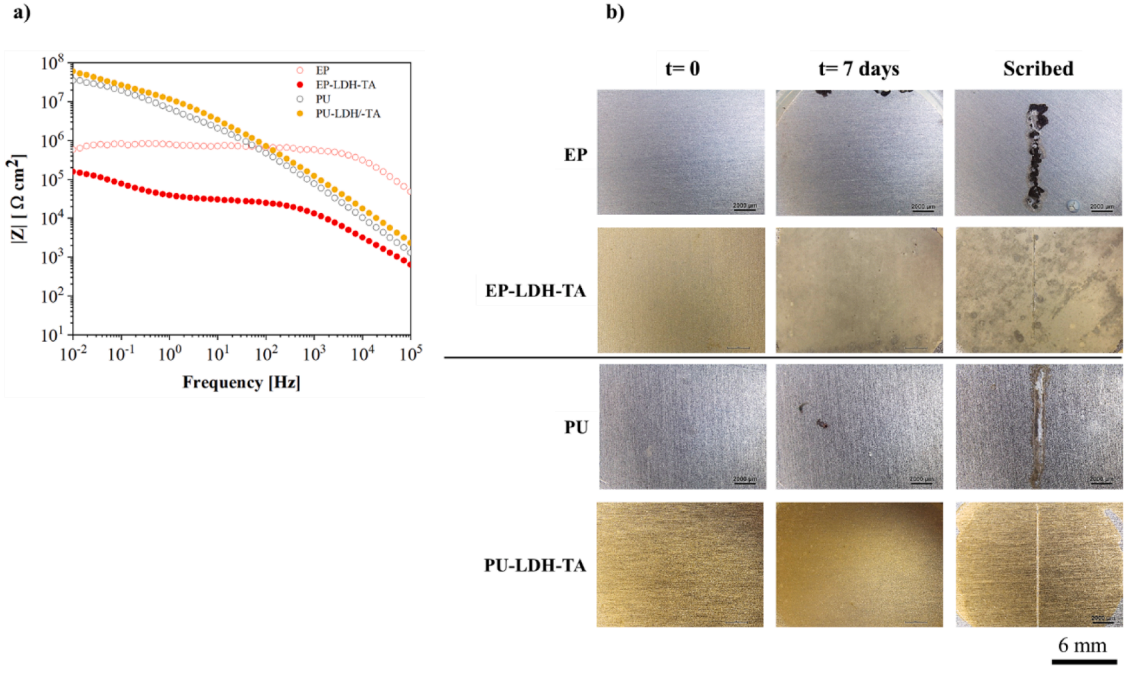

Fig. 5. (a) Bode plot representation of EIS spectra (only impedance magnitude is depicted) and (b) visual inspection of samples (before immersion (t=0), after 7 days of immersion, and scribed sample after 7 days of immersion in 3.5 wt.% NaCl solution) of EP and PU coatings functionalized with the LDH-TA additive at 0.1 wt.%. Note that reference EP and PU coatings images from Figures S2 and S3 were included for reference.

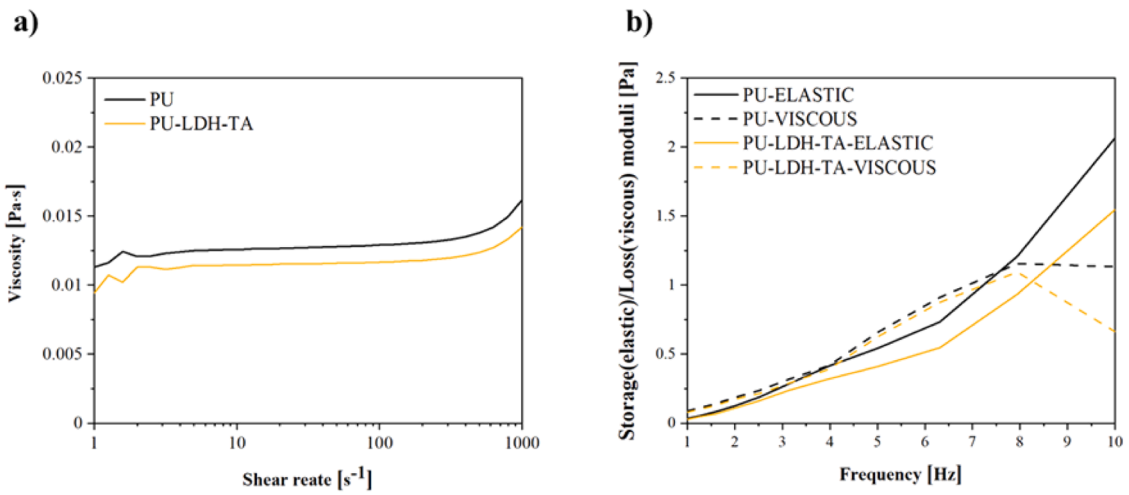

Fig. 6. (a) Rotational and (b) oscillatory rheological properties of PU and PU-LDH-TA formulations.

undesired aggregation effects as reported in prior studies [53,55,56]. Regarding the oscillatory rheological evaluation (Fig. 6**b**), both formulations demonstrate a dominance of the loss modulus (viscous) over the storage modulus (elastic) across almost the entire range of frequencies tested. This indicates a predominantly viscous behaviour, which is beneficial during storage as it counteracts potential sedimentation of the LDH-TA additive [55,57].

Overall, the rheological behaviour of the formulations remains similar, with no significant differences observed, suggesting that the inclusion of 0.1 wt.% LDH-TA does not adversely affect the stability or performance of the PU matrix under the tested conditions. These findings align with other studies in comparable PU formulations where, other additives exhibited similar viscoelastic profiles and sedimentation dynamics [13,14].

3.3.2. Surface properties of PU and PU-LDH-TA coatings

To determine the adhesion of PU and PU-LDH-TA coatings on AA2024 alloy, a qualitative dry adhesion test (ISO 2409) was performed (Fig. 7**a**). The results revealed an excellent dry adhesion (rating of 0) for both coatings. Furthermore, the coating thickness of both PU and PU-LDH-TA coatings was confirmed by optical microscopy, showing a comparable value (Fig. 7**b**; Table 1).

In terms of topographical properties (Fig. 7**c**), PU and PU-LDH-TA coatings showed typical parallel bands along their surface, which are associated with the rolling process of the AA2024-T3 substrate. Additionally, the comparable topographical values (Sa and Ra values: Table 1) confirm the homogeneous application of both coating systems on the AA2024 alloy and the appropriate dispersion of the LDH-TA additive in the PU formulation, without a significant degree of aggregates [53,58]. Another feature is the hydrophobicity of both PU and PU-LDH-TA coatings (Table 1). In this sense, both PU and PU-LDH-TA

Table 1
Summary of thickness, roughness (Ra and Sa), and water contact angle (WCA) values for PU and PU-LDH-TA coatings.

Coating	Thickness [μm]	Ra [μm]	Sa [μm]	WCA [°]
PU	28 ± 3	0.20 ± 0.01	0.40 ± 0.03	85 ± 2
PU-LDH-TA	27 ± 3	0.15 ± 0.01	0.30 ± 0.03	86 ± 2

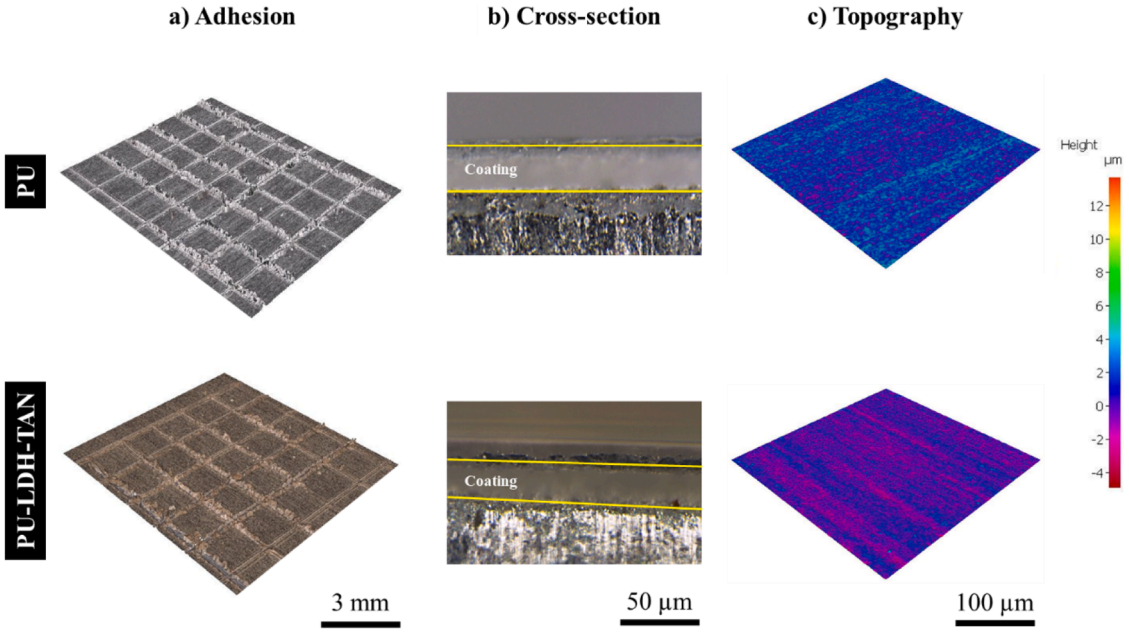

Fig. 7. (a) Adhesion, (b) cross-section view, and (c) optical 3D-topographical maps of the PU and PU-LDH-TA systems.

coatings show low hydrophobicity (<90°), thus indicating that the water interaction with the polyurethane matrix is not affected by the presence of LDH-TA additive [53].

Despite the comparable surface properties between the PU and PU-LDH-TA coatings, FTIR spectra reveal several distinctive features (Fig. 8**a**). Both spectra show the presence of common bands corresponding to the aqueous polyurethane emulsion: (i) the hydroxyl groups stretching at 3400 cm^{-1} and (ii) -C-H (2700 cm^{-1}), C=O and N-H (1100-1800) cm^{-1} from the urethane groups [13,14]. By comparison, the spectrum of the PU coating shows a low-intensity band at ~2270 cm^{-1} corresponding to the isocyanate group (R-NCO). In contrast, the signal intensity of this band was negligible for the PU-LDH-TA coating (Fig. 8**a**). This can be related to the reaction between the hydroxyl groups of the released tannate anions in the emulsion and the isocyanate groups of the hardener [14]. Another difference between both FTIR spectra is the presence of a low-intensity peak at ~ (550-650) cm^{-1} PU-LDH-TA. This peak corresponds to the M-OH stretching (M= Zn, Al) of the LDH-TA structure (Fig. 2).

Regarding the tannate anions release from PU-LDH-TA coating matrix in 3.5 wt.% NaCl solution (Fig. 8**b**), the release increases to 13 mg/L during the first 6 hours. Then, a progressive increase up to ~ 16 mg/L was observed up to the end of the immersion testing. Note that the release of tannate anions from PU is about 30 times smaller than for the LDH-TA powder (recall Fig. 4; *Section 3.1*). This is due to limitations imposed by the coating matrix on the movement of species as compared to the solution [53]. In any case, these results prove that the PU-LDH-TA matrix can release tannate anions in a saline medium.

3.4. Anticorrosion properties of PU and PU-LDH-TA coatings

3.4.1. Corrosion of intact specimens

The long-term corrosion resistance of PU and PU-LDH-TA coatings was evaluated by EIS during 28 days of immersion in 3.5 wt.% NaCl (Fig. 9). As depicted in Bode plots, the electrochemical response of coated substrates can be divided into three distinct regions: (i) the PU coating response at high frequencies (10^3-10^5 Hz); (ii) the aluminium oxide passive layer (10^0-10^3 Hz) and (ii) the electrochemical activity at the substrate interface at low frequencies (10^{-2}-10^0 Hz).

After 1 hour of immersion, the impedance modulus at 10^{-2} Hz (|Z| at 10^{-2} Hz) of the PU-LDH-TA coating ($3{\cdot}10^8$ Ω cm^2) is approximately two orders of magnitude larger than that of the PU coating ($4{\cdot}10^6$ Ω cm^2). Impedance magnitude is also higher in the intermediate/high-frequency range for PU-LDH-TA than for PU, demonstrating the positive effect of the LDH-TA additive against the electrolyte uptake throughout the PU

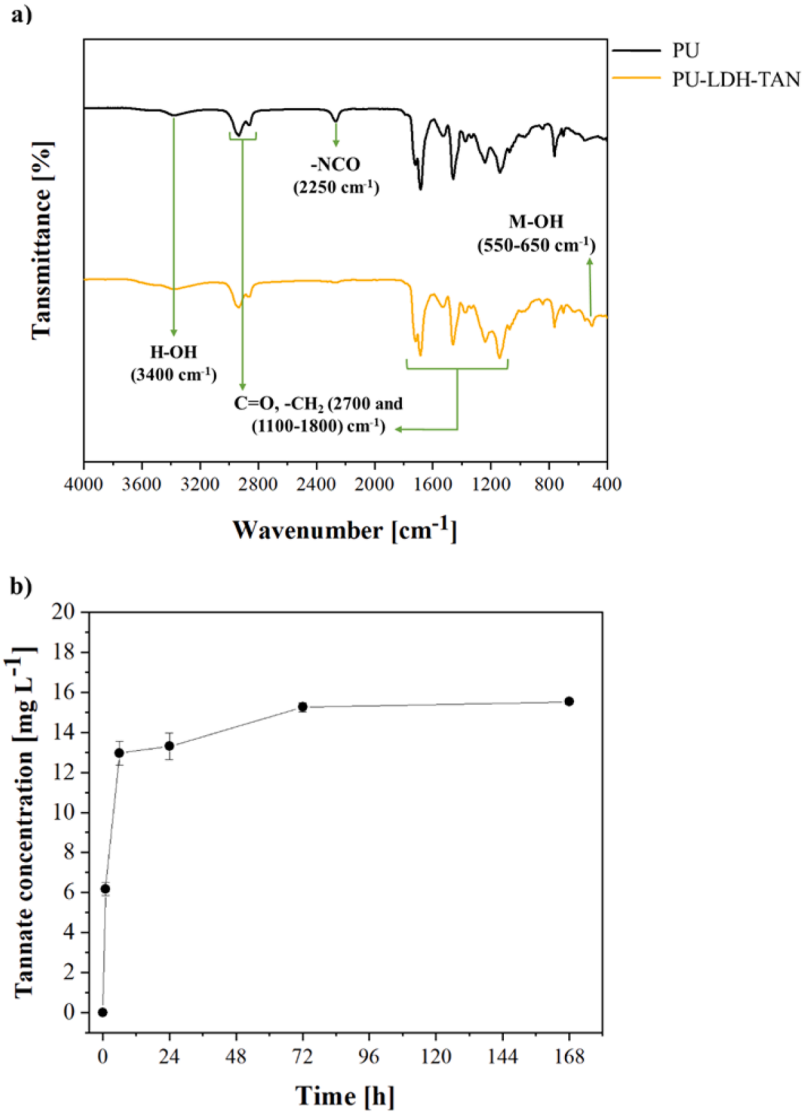

Fig. 8. (a) FTIR spectra of PU and PU-LDH-TA coatings, and (b) release profile of tannate anions per gram of PU-LDH-TA coating in 3.5 wt.% NaCl solution (error bars are standard errors of 3 replicas).

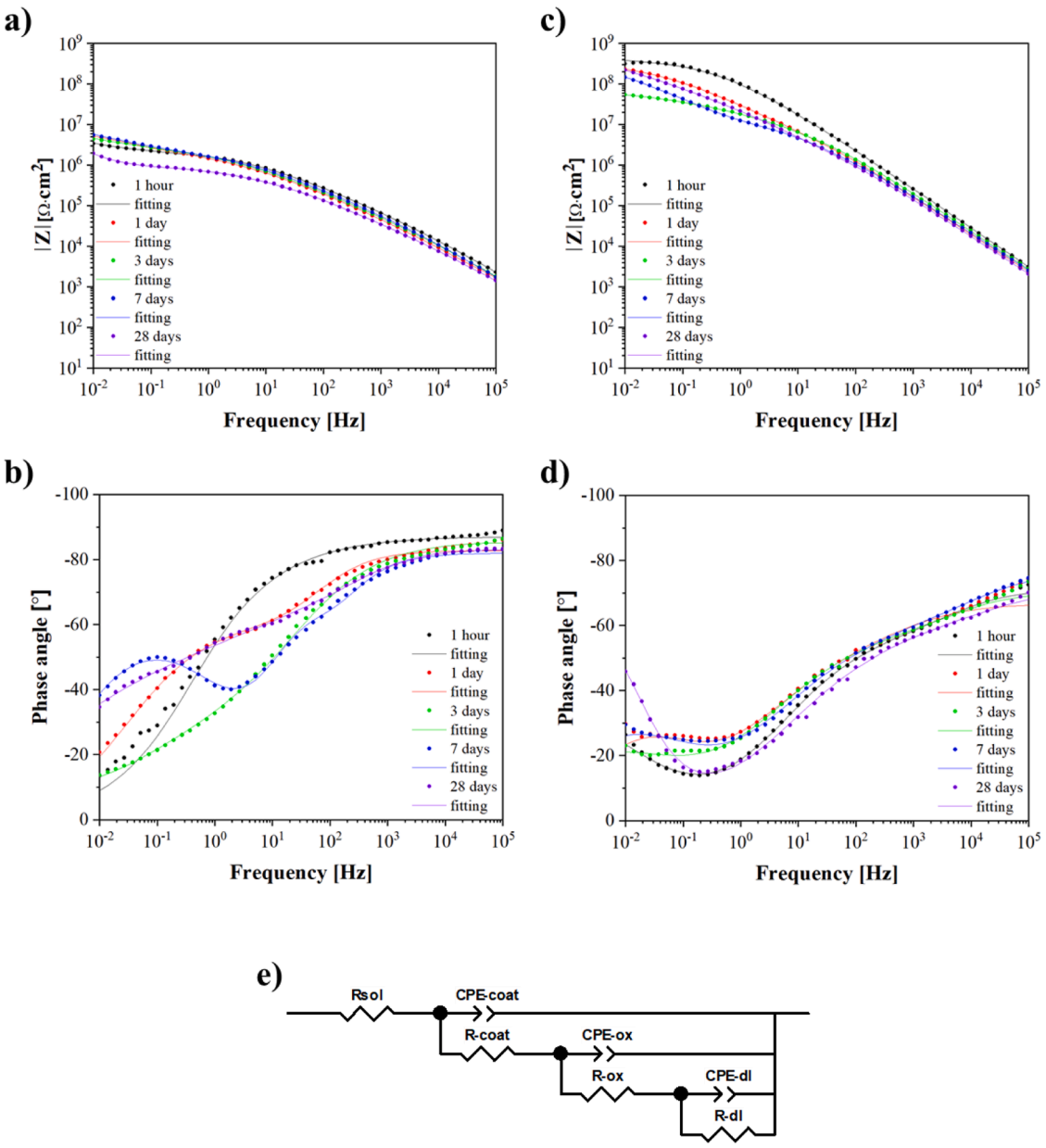

Fig. 9. Bode plots of PU (a, b) and PU-LDH-TA (c, d), and (e) equivalent circuits of PU and PU-LDH-TA coatings after 28 days of immersion time in 3.5 wt.% NaCl solution.

matrix. However, over time, the impedance of PU-LDH-TA systems decreases due to the electrolyte penetration and corrosion processes on the metal surface [14,59]. Despite this behaviour, after 28 days of immersion, the $|Z|$ at 10^{-2} Hz of the PU-LDH-TA coating is more than one order of magnitude higher than that of the PU coating ($\sim 10^{8}$ Ω cm² *vs.* 10^{6} Ω cm²) (Fig. 9**a, c**).

Table 2
Equivalent circuit data for PU and PU-LDH-TA coatings on AA2024 in 3.5 wt.% NaCl solution.

Coating	Time [h]	R-coat [Ω cm²]	Q-coat [S sa cm⁻²]	n_{coat}	C-coat [F cm⁻²]	R-ox [Ω cm²]	Q-ox [S sa cm⁻²]	n_{ox}	C-ox [F cm⁻²]	R-ct [Ω cm²]	Q-dl [S sa cm⁻²]	n_{dl}	C-dl [F cm⁻²]
PU	**1**	$9.5{\cdot}10^{3}$	$1.1{\cdot}10^{-8}$	0.8	$1.1{\cdot}10^{-9}$	$1.0{\cdot}10^{5}$	$1.2{\cdot}10^{-5}$	0.5	$2.6{\cdot}10^{-9}$	$3.1{\cdot}10^{5}$	$1.4{\cdot}10^{-5}$	0.8	$2.2{\cdot}10^{-6}$
	24	$3.7{\cdot}10^{4}$	$3.3{\cdot}10^{-7}$	0.7	$5.0{\cdot}10^{-8}$	$1.8{\cdot}10^{5}$	$1.4{\cdot}10^{-5}$	0.6	$1.4{\cdot}10^{-6}$	$1.1{\cdot}10^{6}$	$8.0{\cdot}10^{-4}$	0.4	$6.4{\cdot}10^{-6}$
	72	$5.6{\cdot}10^{4}$	$2.0{\cdot}10^{-8}$	0.8	$3.6{\cdot}10^{-9}$	$3.0{\cdot}10^{5}$	$1.8{\cdot}10^{-4}$	0.5	$7.2{\cdot}10^{-7}$	$1.5{\cdot}10^{6}$	$1.6{\cdot}10^{-4}$	0.5	$1.3{\cdot}10^{-6}$
	168	$2.3{\cdot}10^{4}$	$3.8{\cdot}10^{-9}$	0.9	$1.4{\cdot}10^{-9}$	$3.0{\cdot}10^{5}$	$1.8{\cdot}10^{-4}$	0.5	$1.3{\cdot}10^{-7}$	$1.6{\cdot}10^{6}$	$2.6{\cdot}10^{-4}$	0.6	$1.4{\cdot}10^{-5}$
	672	$8.2{\cdot}10^{4}$	$1.7{\cdot}10^{-8}$	0.8	$3.4{\cdot}10^{-9}$	$2.5{\cdot}10^{5}$	$7.5{\cdot}10^{-5}$	0.5	$1.3{\cdot}10^{-7}$	$1.8{\cdot}10^{6}$	$1.4{\cdot}10^{-4}$	0.6	$5.1{\cdot}10^{-6}$
PU-LDH-TA	**1**	$1.3{\cdot}10^{4}$	$1.5{\cdot}10^{-8}$	0.9	$5.8{\cdot}10^{-9}$	$7.8{\cdot}10^{7}$	$1.1{\cdot}10^{-6}$	0.9	$1.8{\cdot}10^{-6}$	$4.4{\cdot}10^{8}$	$5.9{\cdot}10^{-3}$	0.5	$1.7{\cdot}10^{-3}$
	24	$3.3{\cdot}10^{4}$	$2.1{\cdot}10^{-8}$	0.9	$9.3{\cdot}10^{-9}$	$1.8{\cdot}10^{6}$	$8.7{\cdot}10^{-6}$	0.8	$2.4{\cdot}10^{-6}$	$1.2{\cdot}10^{8}$	$3.3{\cdot}10^{-3}$	0.5	$5.4{\cdot}10^{-4}$
	72	$6.5{\cdot}10^{4}$	$9.1{\cdot}10^{-9}$	0.9	$4.0{\cdot}10^{-9}$	$4.6{\cdot}10^{6}$	$1.2{\cdot}10^{-5}$	0.8	$3.9{\cdot}10^{-6}$	$9.2{\cdot}10^{7}$	$5.7{\cdot}10^{-3}$	0.6	$2.5{\cdot}10^{-4}$
	168	$2.6{\cdot}10^{4}$	$4.7{\cdot}10^{-9}$	0.9	$1.7{\cdot}10^{-9}$	$8.2{\cdot}10^{6}$	$7.5{\cdot}10^{-7}$	0.8	$1.3{\cdot}10^{-7}$	$3.7{\cdot}10^{8}$	$1.2{\cdot}10^{-3}$	0.7	$1.9{\cdot}10^{-4}$
	672	$9.3{\cdot}10^{4}$	$4.3{\cdot}10^{-8}$	0.8	$1.1{\cdot}10^{-8}$	$6.2{\cdot}10^{6}$	$1.8{\cdot}10^{-3}$	0.5	$1.6{\cdot}10^{-4}$	$1.8{\cdot}10^{8}$	$2.4{\cdot}10^{-3}$	0.4	$2.9{\cdot}10^{-4}$

To further analyze the Bode diagrams as a function of immersion time, equivalent circuits with 3 time constants were used to fit the experimental data (Fig. 9**e**). The selection of an equivalent circuit was performed considering the number of time constants detected in the EIS spectra and based on similar studies described in the literature [60,61]. The electrochemical parameters obtained are presented in Table 2.

Rsol represents the electrolyte resistance (20-50 Ω cm^2). As the fitted CPE parameter (Q) does not represent the dimensions of real capacitance, it was converted to a real capacitance (C; Table 2) using the Equations 1-2. In short, C-coat/R-coat are the capacitive and resistive behaviour of the PU layer. C-ox/R-ox is attributed to the capacitive and resistive behaviour of the native aluminium oxide layer. Finally, C-dl/R-ct is attributed to the double-layer capacitance of the electrolyte/metal interface and the charge transfer resistance.

Table 2 shows that both coatings exhibit a similar order of magnitude in R-coat and C-coat, indicating comparable long-term resistance of the outer layer when LDH-TA is included in the PU coating. Over time, all the C and Q elements tend to similarly increase, which is typically attributed to increased water uptake of the PU matrix [62,63]. In this sense, although the PU-LDH-TA coating displays higher C-ox/C-dl values, the increase in R-ox/R-ct confirms its superior corrosion resistance. This result is in agreement with the active corrosion protection effect rendered by TA, reported recently by our group [12]. This, in turn, can be rationalized as being due to (i) the improved barrier effect provided by the LDH-TA additive and (ii) the release of tannates from the LDH structure when the corrosion process occurs.

3.4.2. Active corrosion assessment of scribed PU and PU-LDH-TA coatings

The active corrosion protection of the PU-LDH-TA coating was evaluated first as a point-shaped defect and then as a linear scribe. The point defect was first evaluated during 7 days of immersion in a 3.5 wt.% NaCl solution, with the PU as reference (**Figure S5**). Initially, the impedance modulus was measured after one hour of immersion for both coatings. Then, after the artificial point-shaped defect, the decrease in impedance was more significant for PU than for PU-LDH-TA. In the end, a difference of around one order of magnitude higher for the PU-LDH-TA system was observed.

As can be seen in the SEM/EDS analysis after immersion of both

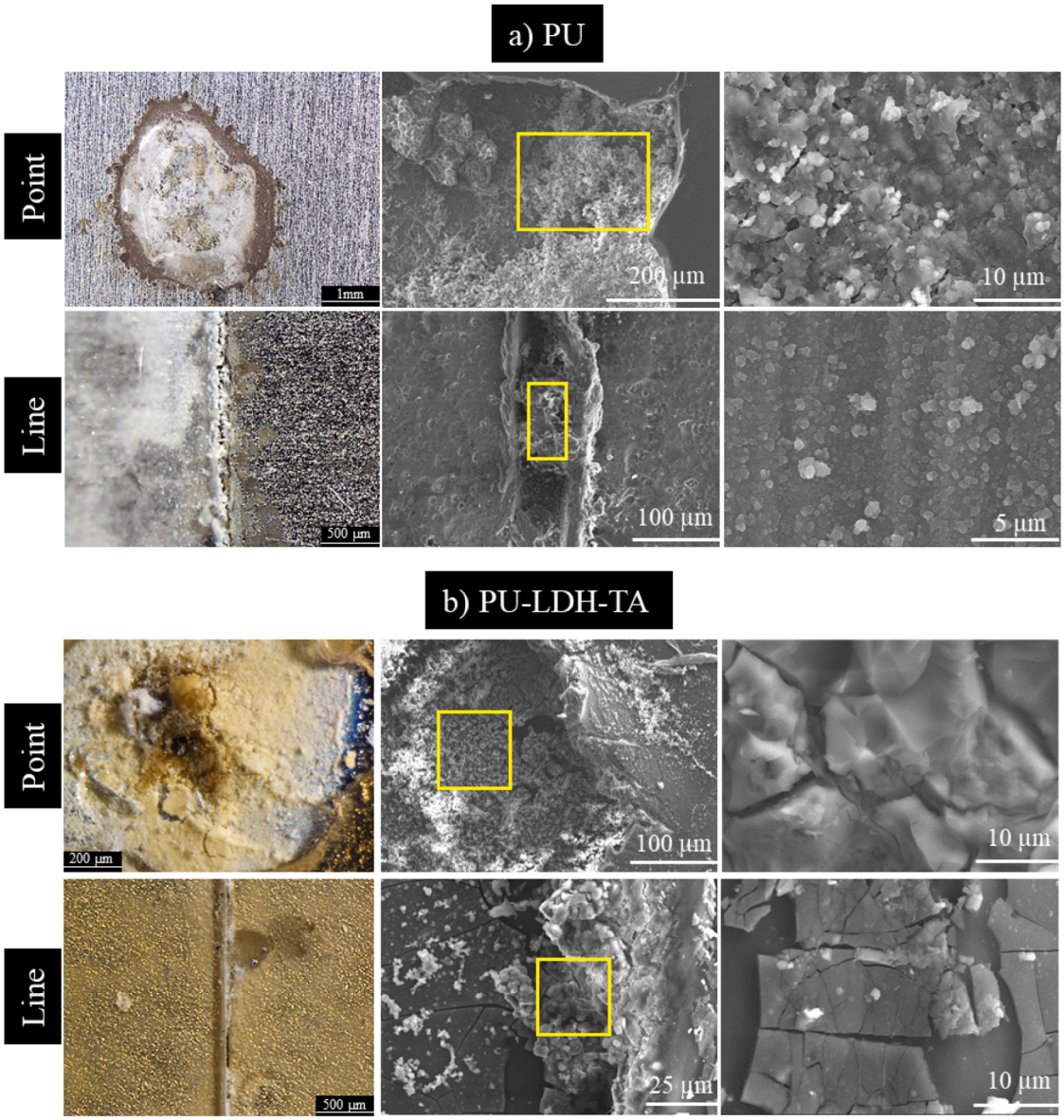

Fig. 10. Longitudinal scanning optical and electron micrographs corresponding to the point- and linear-shaped defects of (a) PU and (b) PU-LDH-TA coatings on AA2024 alloy after 7 days of immersion in 3.5 wt.% NaCl solution. Yellow squares indicate areas where EDS analysis was performed.

point-shaped (after EIS; **Figure S5**) and linear-shaped defects (Fig. 10), the enhanced integrity of the PU-LDH-TA coating resulted in the formation of a homogeneous, slightly brown-coloured oxide layer in the artificially inflicted defects. According to the authors' previous study on the inhibition mechanism of tannate anions in the AA2024 alloy [12], the brown colour of the corrosion product layer resembles the presence of Al-tannate species for bare alloy AA2024 alloy exposed to tannic acid-based solutions [12]. This phenomenon likely restricts the diffusion of chloride anions to the metallic substrate, thereby delaying further corrosion progression. As expected, the defect in the PU coating shows a corrosion product layer similar to the corrosion of the AA2024 alloy itself (Fig. 10**a**), *i.e.*, the formation of aluminium hydroxides as corrosion products, possibly bayerite (β-$Al(OH)_3$) [64].

The EDS analysis (Table 3) in the marked areas of Fig. 10 reveals a higher concentration of Al in the defect formed on the PU coating compared to the PU-LDH-TA coating. This may be due to a higher content of Al (hydro)oxide compounds in the defects of the PU coating [64]. Another feature is the higher C content in the PU-LDH-TA coating (~ 46-61 at.%) compared to the PU coating (~ 38-39 at.%). As expected, this is in line with (i) the release and precipitation of tannate from the PU-LDH-TA coating (Fig. 8**b**) on the bare substrate, and (ii) the higher impedance achieved in the EIS test (**Figure S5**). The presence of Cu and Mg can be associated with the presence of intermetallics on the AA2024 alloy. The presence of Na and Cl signals can be associated with traces of NaCl after the immersion test.

To better quantify the self-healing ability of the PU-LDH-TA coating in the presence of defects, Fig. 11 shows surface images and SVET maps of PU and PU-LDH-TA coatings with two defects at the beginning of immersion and after 6 h and 24 h of immersion in 0.05M NaCl solution. The anodic activity (from metal oxidation; red) corresponds to positive currents, while the cathodic activity (reduction of oxygen or water; blue) corresponds to negative currents. The green colour corresponds to zero-current regions (zero z-component of current density).

In the case of PU coating (Fig. 11**a**), no current density in the first minutes of immersion was detected, possibly due to the lack of enough current to be detectable by the SVET microelectrode. Then, the current increased, and the corrosion was confined to the two defects (no activity was detected outside the defects in any of the tested samples). As expected, one defect was anodic (red dot) and the other was cathodic (blue dot). This separation of corrosion activity in cathodic and anodic defects is usually noticed in scribed-coated metals [65].

In the case of PU-LDH-TA coating (Fig. 11**a**), the corrosion onset started at the beginning of the immersion. However, the currents disappeared after 6 hours of immersion, thereby indicating an active corrosion protection effect. To better analyze these two different trends, Fig. 11**b** shows the evolution of the currents in both defects over time. The PU-LDH-TA sample shows minimal corrosion activity at the beginning of immersion (2 μA cm^{-2}) and the subsequent decrease after 10 hours of immersion.

This inhibition performance can be associated with the release of tannate anions from the LDH-TA additive dispersed in the coating. During the release study of tannate anions from the PU-LDH-TA coating (Fig. 8**b**, *Section 3.3.2*), a substantial and sustained release of tannate anions was detected, beginning immediately at the onset of the study and persisting till the end of the study. This may justify the lower anodic/cathodic currents detected from the first minutes of immersion of the PU-LDH-TA coating (Fig. 11).

On this basis, the self-healing ability of the PU-LDH-TA coating in NaCl medium can be interpreted by combining the findings of the present work and the fundamentals of tannic acid inhibition discussed in [12]. In short, once the release of tannate anions from the coating PU matrix occurs, the tannate anions are chemisorbed in the Al matrix and the Cu-rich secondary phases [12]. As corrosion progresses, the resultant oxide layer can be defined as a mixture of tannate and aluminium hydroxides, as reported in [12] and likewise confirmed in the SEM/EDS analysis of the defected areas after corrosion (Fig. 10**b**; Table 3).

Besides, although the tannate anion release is hardly detectable in the tested PU-LDH-TA coatings, the study of R. del Olmo *et al.* [12] demonstrated that the low concentration of tannate anions (0.1-1 mM) in NaCl medium results in an oxide layer with improved stability and long-term corrosion protection than that formed in more concentrated solutions. Therefore, the present findings demonstrate that, even at low concentrations, the tannate anion released from the PU-LDH-TA coating ensures the active corrosion protection ability after physical damage of the coating in NaCl solution. A representative illustration of this mechanism is included in **Figure S6**.

Table 3
EDS (at.%) area analysis of point- and linear-shaped defects formed on PU and PU-LDH-TA coatings on AA2024 alloy after 7 days of immersion in 3.5 wt.% NaCl solution.

Coating	Location	Element [at.%]						
		C	O	Al	Cl	Na	Mg	Cu
PU	Point	39.5	39.2	20.6	0.2	-	0.3	0.2
	Line	38.1	31.7	29.3	0.1	-	0.4	0.4
PU-LDH-TA	Point	61.4	34.7	3.5	0.3	0.1	-	-
	Line	46.1	45.3	7.9	0.6	0.1	-	-

4. Conclusions and future perspectives

The main conclusions regarding the formation, characterization, and corrosion performance of the Tannic- and LDH-TA-containing, water-based epoxy and polyurethane coatings applied onto AA2024 alloy can be summarized as follows:

- Short-term corrosion (EIS) results reveal that direct incorporation of TA incorporation into EP coatings leads to low corrosion performance and heterogeneous surface appearance, regardless the coating is intact or scribed. Besides, negative effects of adding TA to PU were also found in terms of coating adhesion.
- Tannate anions adsorption/loading in LDH was successfully confirmed, regardless of the intercalation pH (6, 8, and 10). The release study of tannate anions in a saline medium shows their burst release right after immersion, thus effectively inhibiting the corrosion progress of the AA2024 alloy. The extent of TA released suggests that at least part of intercalated TA can be released by anion exchange.
- The LDH-TA additive in PU results in improved integrity when the coating is scratched. By contrast, the addition of LDH-TA in the EP matrix did not improve the protective properties concerning the reference EP.
- The release study of tannate anions from the PU-LDH-TA coating shows a slower release compared to the LDH-TA powder due to the low permeability/mobility of species through the PU matrix *vs.* solution.
- Rheological studies, surface characterization, and electrochemical tests revealed that the incorporation of LDH-TA into the PU matrix (PU-LDH-TA) not only preserves its structural properties but also provides enhanced corrosion protection in the saline medium.
- Microstructural analysis of the scratched PU-LDH-TA coating after 7 days of immersion in saline medium revealed the formation of a brown-coloured oxide layer with a significant C content. This confirms (i) the release of tannate anions from the PU coating to the defect and (ii) the chemisorption-formation of a corrosion-resistant layer composed of tannate and aluminium hydroxides.
- The SVET analysis reveals that the measured anodic and cathodic currents in the defects of the PU-LDH-TA coating were lower than those of the reference PU coating, thus proving its active corrosion protection performance.

The present findings reveal that the use of water-based polyurethane,

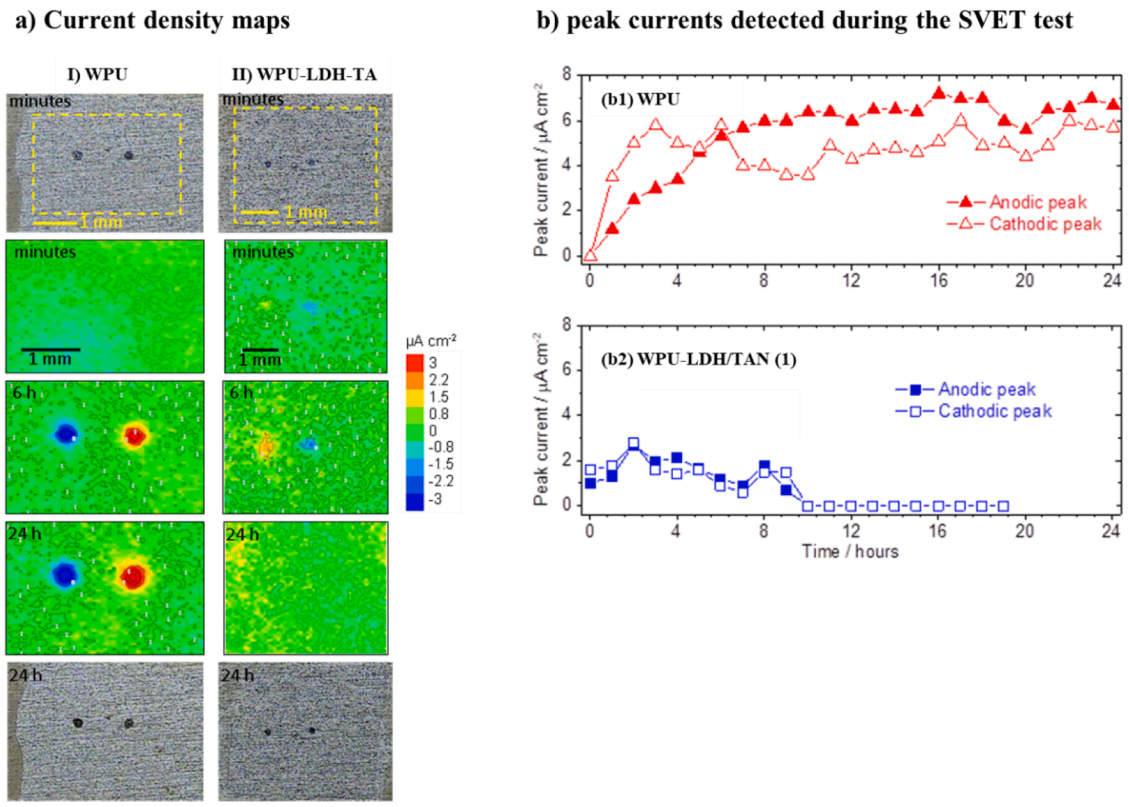

Fig. 11. a) Surface images and SVET maps of PU, and PU-LDH-TA coatings on AA2024-T3 measured at the beginning of immersion, and after 6 and 24 hours of immersion in 0.05 M NaCl with two defects, and b) anodic and cathodic peak currents measured during the first 24 hours of immersion, 100 μm above the two defects on PU, and PU-LDH-TA coatings.

Zn-Al-LDH, and tannic acid in the synthesis of the PU-LDH-TA coating can be considered a promising Cr(VI)-free alternative for AA2024 alloy in the aircraft industry. However, it is worth mentioning that further studies on mechanical performance and scaling up should be carried out in the future to meet the stringent requirements of the aircraft industry.

CRediT authorship contribution statement

Rubén del Olmo: Writing – review & editing, Writing – original draft, Visualization, Validation, Software, Project administration, Methodology, Investigation, Funding acquisition, Formal analysis, Data curation, Conceptualization. **Cristina Neves:** Writing – review & editing, Visualization, Validation, Methodology, Formal analysis, Data curation. **Alexandre Bastos:** Writing – review & editing, Visualization, Validation, Software, Investigation, Formal analysis, Data curation. **Raúl Arrabal:** Writing – review & editing, Visualization, Validation, Supervision, Resources, Project administration, Investigation, Funding acquisition, Formal analysis. **João Tedim:** Writing – review & editing, Visualization, Validation, Supervision, Resources, Project administration, Funding acquisition, Formal analysis, Conceptualization.

Declaration of competing interest

The authors declare that they have no known competing financial interests or personal relationships that could have appeared to influence the work reported in this paper.

Acknowledgements

This work was developed within the scope of Project CICECO-Aveiro Institute of Materials (UIDB/50011/2020, UIDP/50011/2020, and LA/P/0006/2020), financed by national funds through the FCT/MEC (PIDDAC). R. del Olmo acknowledges the financial support from the Margarita Salas CT18/22 postdoctoral grant. A. Bastos and C. Neves are funded by national funds (OE), through FCT - Fundação para a Ciência e a Tecnologia, I.P., in the scope of the framework contract foreseen in the numbers 4, 5, and 6 of article 23, of the Decree-Law 57/2016, of August 29, changed by Law 57/2017, of July 19. R. Arrabal acknowledges the support by PID2021-124341OB-C22/AEI/10.13039/501100011033/FEDER, UE (MICIU).

Supplementary materials

Supplementary material associated with this article can be found, in the online version, at doi:10.1016/j.surfin.2025.106800.

Data availability

The raw/processed data required to reproduce these findings cannot be shared at this time as the data also forms part of an ongoing study.

References

[1] Visser, P., H. Terryn, and J.M.C. Mol, *Aerospace coatings*, in *Springer Series in Materials Science*. 2016. p. 315-372.
[2] K.K. Sankaran, R.S. Mishra, in: K.K. Sankaran, R.S. Mishra (Eds.), *Chapter 4 - Aluminum Alloys*, in *Metallurgy and Design of Alloys with Hierarchical Microstructures*, Elsevier, 2017, pp. 57–176.
[3] K.A. Yasakau, M.L. Zheludkevich, M.G.S. Ferreira, 15 - Role of intermetallics in corrosion of aluminum alloys. Smart corrosion protection, in: R. Mitra (Ed.), Intermetallic Matrix Composites, Woodhead Publishing, 2018, pp. 425–462.
[4] C. Vargel, Chapter F.1 - Protection of aluminium, in: C. Vargel (Ed.), Corrosion of Aluminium (Second Edition), Elsevier, Amsterdam, 2020, pp. 383–443.
[5] *LANXESS Deutschland GmbH Ltd. Surface treatment for applications in the aeronautics and aerospace industries, unrelated to Functional chrome plating or Functional chrome plating with decorative character.* 2019.
[6] O. Gharbi, et al., Chromate replacement: what does the future hold? NPJ Mater. Degradat. 2 (1) (2018) 12.

[7] P. Visser, H. Terryn, J.M.C. Mol, Active corrosion protection of various aluminium alloys by lithium-leaching coatings, Surface Interface Anal. 51 (12) (2019) 1276–1287.

[8] J. Mardel, et al., The characterisation and performance of Ce(dbp)3-inhibited epoxy coatings, Progress Organic Coat. 70 (2) (2011) 91–101.

[9] Y. Hu, et al., A bifunctional epoxy coating doped by cerium (III)-8-hydroxyquinoline: Early self-reporting and stimuli-responsive inhibition on corrosion of Al substrate, Progress Organic Coat. 182 (2023) 107616.

[10] D. Snihirova, et al., Comparison of the synergistic effects of inhibitor mixtures tailored for enhanced corrosion protection of bare and coated AA2024-T3, Surface Coat. Technol. 303 (2016) 342–351.

[11] S.V. Lamaka, et al., Comprehensive screening of Mg corrosion inhibitors, Corros. Sci. 128 (2017) 224–240.

[12] R. del Olmo, et al., Corrosion inhibitor from nature: Fundamentals of tannic acid inhibition for AA2024 alloy, Appl. Surface Sci. 680 (2025) 161434.

[13] A. Sushkova, et al., A novel smart coating with hexacyanoferrate intercalated layered double hydroxides nanoadditive for early detection of carbon steel corrosion, Front. Chem. Eng. 5 (2023).

[14] T.L.P. Galvão, et al., Improving the functionality and performance of AA2024 corrosion sensing coatings with nanocontainers, Chem. Eng. J. 341 (2018) 526–538.

[15] H. Yan, et al., Synergistic mechanism of ternary green corrosion inhibitors for N80 steel in 20 wt% HCl solution: Encapsulation and transportation of vanillin through micelles formed by ionic liquids, Corros. Sci. 227 (2024) 111750.

[16] D. Venkatachalam, et al., Smart release of turmeric as a potential corrosion inhibitor from a pH-responsive polymer encapsulated highly ordered mesoporous silica containers, Surf. Interfaces 45 (2024) 103883.

[17] X. Ji, et al., Developing wide pH-responsive, self-healing, and anti-corrosion epoxy composite coatings based on encapsulating oleic acid/2-mercaptobenzimidazole corrosion inhibitors in chitosan/poly(vinyl alcohol) core-shell nanofibers, Progress Organic Coat. 161 (2021) 106454.

[18] Y. Guo, et al., Preparation of self-healing superhydrophobic polyacrylate coatings based on silica matrix-microcapsules containing corrosion inhibitor for long-term corrosion protection, Progress Organic Coat. 188 (2024) 108267.

[19] A. Versteg, et al., Improving the barrier properties of chitosan coatings through Schiff base formation and halloysite incorporation for corrosion protection of commercially pure aluminum (cp-Al), Mater. Today Commun. 38 (2024) 108046.

[20] Y. Yang, Y. Chen, Fabrication of dual self-healing silane nanocomposite for efficient corrosion protection of aluminum alloy, J. Alloys Compounds 983 (2024) 173890.

[21] W. Bai, et al., Intelligent anti-corrosion coating with multiple protections using active nanocontainers of ZnAl LDH equipped with ZIF-8 encapsulated environment-friendly corrosion inhibitors, Progress Organic Coat. 185 (2023) 107940.

[22] R. Marathe, et al., Neem acetylated polyester polyol—Renewable source based smart PU coatings containing quinoline (corrosion inhibitor) encapsulated polyurea microcapsules for enhance anticorrosive property, Ind. Crops Products 77 (2015) 239–250.

[23] A.C. Bouali, et al., Layered double hydroxides (LDHs) as functional materials for the corrosion protection of aluminum alloys: A review, Appl. Mater. Today 21 (2020) 100857.

[24] Y. Cao, et al., Layered double hydroxide (LDH) for multi-functionalized corrosion protection of metals: A review, J. Mater. Sc. Technol. 102 (2022) 232–263.

[25] D.A. Leal, et al., Layered materials as nanocontainers for active corrosion protection: A brief review, Appl. Clay Sci. 225 (2022) 106537.

[26] M. Tabish, et al., Reviewing the current status of layered double hydroxide-based smart nanocontainers for corrosion inhibiting applications, J. Mater. Res. Technol. 10 (2021) 390–421.

[27] J. Tedim, et al., Layered double hydroxides for corrosion-related applications—Main developments from 20 years of research at CICECO, Front. Chem 10 (2022).

[28] M. Adampourezare, B. Nikzad, Layered double hydroxide nanoparticles as signal-amplification elements in DNA biosensors: Recent progress and challenges, Microchem. J. 199 (2024) 110151.

[29] V.K. Ameena Shirin, et al., Advanced drug delivery applications of layered double hydroxide, J. Controll. Release 330 (2021) 398–426.

[30] M. Pavlovic, et al., Surface modification of two-dimensional layered double hydroxide nanoparticles with biopolymers for biomedical applications, Adv. Drug Del. Rev. 191 (2022) 114590.

[31] K.A. Yasakau, et al., A novel bilayer system comprising LDH conversion layer and sol-gel coating for active corrosion protection of AA2024, Corros. Sci. 143 (2018) 299–313.

[32] A.C. Bastos, et al., Review—on the application of the scanning vibrating electrode technique (SVET) to corrosion research, J. Electrochem. Soc. 164 (14) (2017) C973.

[33] A.C. Bastos, M.G.S. Ferreira, et al., 1 - Application of the scanning vibrating electrode technique to the characterization of modern coatings, in: M. Aliofkhazraei, et al. (Eds.), Handbook of Modern Coating Technologies, ElsevierAmsterdam, 2021, pp. 1–43.

[34] X. Fei, et al., Tannic acid as a bio-based modifier of epoxy/anhydride thermosets, Polymers 8 (2016) 314, https://doi.org/10.3390/polym8090314.

[35] J.V. Nardeli, et al., Novel healing coatings based on natural-derived polyurethane modified with tannins for corrosion protection of AA2024-T3, Corros. Sci. 162 (2020) 108213.

[36] J. Tedim, et al., Zn–Al layered double hydroxides as chloride nanotraps in active protective coatings, Corros. Sci. 55 (2012) 1–4.

[37] T. Taher, et al., A comparative study on the adsorption behavior of congo red on to Znal and Zncr layered double hydroxides, J. Pure Appl. Chem. Res. 9 (2020) 108–116.

[38] A.N. Salak, et al., Anion exchange in Zn–Al layered double hydroxides: In situ X-ray diffraction study, Chem. Phys. Lett. 495 (1) (2010) 73–76.

[39] Neves, C.S., et al., *Layered double hydroxide clusters as precursors of novel multifunctional layers: a bottom-up approach.* 2019. 9(5): p. 328.

[40] M. Shabanian, M. Hajibeygi, A. Raeisi, 2 - FTIR characterization of layered double hydroxides and modified layered double hydroxides, in: S. Thomas, S. Daniel (Eds.), Layered Double Hydroxide Polymer Nanocomposites, Woodhead Publishing, 2020, pp. 77–101.

[41] A.C. Bouali, et al., Mechanism of LDH direct growth on aluminum alloy surface: a kinetic and morphological approach, J. Phys. Chem. C 125 (21) (2021) 11687–11701.

[42] J.T. Kloprogge, R.L. Frost, Fourier transform infrared and raman spectroscopic study of the local structure of Mg-, Ni-, and Co-Hydrotalcites, J. Solid State Chem. 146 (2) (1999) 506–515.

[43] J. Tedim, et al., Influence of preparation conditions of Layered Double Hydroxide conversion films on corrosion protection, Electroch. Acta 117 (2014) 164–171.

[44] T. Wahyono, et al., Fourier Transform Mid-Infrared (FTIR) Spectroscopy to Identify Tannin Compounds in The Panicle of Sorghum Mutant Lines, IOP Conf. Ser. Mater. Sci. Eng. 546 (2019) 042045.

[45] K. Ranoszek-Soliwoda, et al., The role of tannic acid and sodium citrate in the synthesis of silver nanoparticles, J. Nanopart. Res. 19 (8) (2017) 273.

[46] A. Kuznetsova, et al., Antimicrobial activity of 2-mercaptobenzothiazole released from environmentally friendly nanostructured layered double hydroxides, J. Appl. Microbiol. 122 (5) (2017) 1207–1218.

[47] Y. Dong, F. Wang, Q. Zhou, Protective behaviors of 2-mercaptobenzothiazole intercalated Zn-Al-layered double hydroxide coating, J. Coat. Technol. Res. 11 (5) (2014) 793–803.

[48] M. Tabish, et al., Improving the corrosion protection ability of epoxy coating using CaAl LDH intercalated with 2-mercaptobenzothiazole as a pigment on steel substrate, Progress Organic Coat. 165 (2022).

[49] S. Fang, et al., Preparation of gallic acid intercalated layered double hydroxide for enhanced corrosion protection of epoxy coatings, Coatings 13 (1) (2023).

[50] J. Wang, et al., A comparative experimental and theoretical calculation study of CaAl-LDH modified with various aromatic inhibitors for corrosion protection study in epoxy coatings, Corros. Sci. 231 (2024).

[51] M. Kotal, S.K. Srivastava, Synergistic effect of organomodification and isocyanate grafting of layered double hydroxide in reinforcing properties of polyurethane nanocomposites, J. Mater. Chem. 21 (46) (2011) 18540–18551.

[52] S. Guo, et al., Structural characterization, thermal and mechanical properties of polyurethane/CoAl layered double hydroxide nanocomposites prepared via in situ polymerization, Compos. Sci. Technol. 71 (6) (2011) 791–796.

[53] L. van Tonder, F.J. Labuschagné, Systematic Literature Review of the Effect of Layered Double Hydroxides on the Mechanical Properties of Rubber, Polymers 13 (2021), https://doi.org/10.3390/polym13213716.

[54] M. Kotal, S.K. Srivastava, A.K. Bhowmick, Thermoplastic polyurethane and nitrile butadiene rubber blends with layered double hydroxide nanocomposites by solution blending, Polymer Int. 59 (1) (2010) 2–10.

[55] R.A. Bhavsar, K.M. Nehete, Rheological approach to select most suitable associative thickener for water-based polymer dispersions and paints, J. Coat. Technol. Res. 16 (4) (2019) 1089–1098.

[56] R. Arrigo, et al., An insight into the interaction between functionalized thermoplastic elastomer and layered double hydroxides through rheological investigations, Composites Part B Eng. 139 (2018) 47–54.

[57] E. Orgilés-Calpena, et al., Effect of annealing on the properties of waterborne polyurethane adhesive containing urethane-based thickener, Int. J. Adhesion Adhes. 29 (8) (2009) 774–780.

[58] J. Chang, et al., Synthesis and characterization of environmentally-friendly self-matting waterborne polyurethane coatings, Coatings 10 (2020), https://doi.org/10.3390/coatings10050494.

[59] M.L. Zheludkevich, et al., On the application of electrochemical impedance spectroscopy to study the self-healing properties of protective coatings, Electrochem. Commun. 9 (10) (2007) 2622–2628.

[60] R. del Olmo, et al., Hybrid PEO/sol-gel coatings loaded with Ce for corrosion protection of AA2024-T3, Progress Organ. Coat. 182 (2023) 107667.

[61] R. del Olmo, et al., Hybrid sol-gel coatings applied on anodized AA2024-T3 for active corrosion protection, Surface Coat. Technol. 419 (2021) 127251.

[62] Y. Li, et al., Self-aligned graphene as anticorrosive barrier in waterborne polyurethane composite coatings, J. Mater. Chem. A 2 (34) (2014) 14139–14145.

[63] G. Cai, et al., Polydopamine-wrapped carbon nanotubes to improve the corrosion barrier of polyurethane coating, RSC Adv. 8 (42) (2018) 23727–23741.

[64] G. Lefèvre, et al., Hydration of γ-Alumina in Water and Its Effects on Surface Reactivity, Langmuir 18 (20) (2002) 7530–7537.

[65] A.C. Bastos, M.C. Quevedo, M.G.S. Ferreira, Investigating the separation of anodic and cathodic defects in organic coatings applied on metal substrates. An experimental contribution, Progress Organ. Coat. 96 (2016) 26–31.